[6] Bakhtar, F., Mohammadi Tochai, M.T., "An investigation of two-dimensional flows of nucleating and wet steam by the time-marching method. "Int. J.Heat and Fluid Flow, 5-18. 1980.
[7] Bakhtar, F., Bamkole, B.O., "An examination of the throughflow of steam in a turbine stage by a time-marching method." Proc. Instn Mech. Engrs, Part A, 233-243. 1989.
[8] Yeoh, C.C., Young, J.B., "Non-equilibrium throughflow analyses of low-pressure wet steam turbines." Trans. ASME, J. Engng for Gas Turbines and power, 716-724. 1984.
[9] Young, J.B., "two-dimensional Non-equilibrium wet steam calculations for nozzles and turbines cascades." Trans. ASME, J. Turbomachinery, 569-579. 1992.
[10] Bakhtar, F., Mahpeykar, M.R., K.K.Abbas., "An investigation of nucleating flows of steam in a cascade of turbine blading - theoretical treatment." Transactions of the ASME. Vol.117,1995.
[11] Bakhtar, F., Mahpeykar, M.R., "On the performance of a cascade of turbine rotor tip section blading in nucleating steam." ImechE ,vol. 211, part C ,1997
[12] Moheban, M., Young, J.B., "A time-marching method for the calculation of blade-to-blade non- equilibrium wet steam flows in turbine cascades." C76/84 ImechE 1984.
[13] Subramanina, S.V., Bozzola, R., "Application of Runge Kutta time marching scheme for the computation of transonic flows in turbomachines." AIAA, propulsion conference, July 1985.
[14] Mahpeykar, M.R., Noroozi, Z.,Teymourtash, A.R., "An investigation of two phase flow in a supersonic one dimensional nozzle and increasing the speed of solving of droplet growth equations." Journal of Iranian Mechanical Engineering, No. 4/122. Spring 2000.
[15] Martinelli, L., "Calculations of viscous flows with a multigrid method". Ph.D. Thesis, Princeton University. 1987.
[16] Dick, E., "Introduction to finite volume techniques.", V.K.I Lecture series. 1990
[17] Swanson, R.C., Radespiel, R., "Cell center and cell vertex multigrid scheme for the Navier Stokes equations." AIAA Journal, May 1991.
[18] Mahpeykar, M.R., Teymourtash, A.R., "A fast and accurate Range Kutta time marching scheme including refinement of turbine cascade." In proceeding of the Ninth Asian Congress of Fluid Mechanics (9ACFM), (IUT, Isfahan, Iran), May 2002.
[19] Jameson, A., Schmidt, W., and Turkel, E., "Numerical solution of Euler equations by finite volume method using Runge Kutta time-stepping scheme."AIAA paper, 81-1259, June 1981.
[20] Gostelow, J.P.,"Cascade aerodynamics." pergamon, 1984.
[21] Skillings, S.A., "Condensation phenomena in a turbine blade passage.", j. Fluid Mech. vol. 200, pp. 409-424, 1989.
[22] Bakhtar, F., Webb, R.A., Shojaee-fard, M.H. Siraj, M.A. "An investigation of nucleating flows of steam in a cascade of turbine blading." Transactions of the ASME. Vol. 115, 1993.
[23] Frenkel, J., "Kinetic theory of liquids" (Oxford University Press), 1946.
[24] MacDonald, J.E., "Homogeneous nucleation of vapour condensation" Am. J. Phys. 817-870, 1962-63.
[25] Gerber, A.G., "Two-phase Eulerian/Lagrangian Model for Nucleating Steam Flow" Journal of Fluid Eng. Vol. 124.Issue 2 , PP.465-475 June 2002.
[26] Courtney, W.A., "Remarks on homogeneous nucleation" J.Chem. Phys., 35, 2249, 1961.
[27] Kantrowitz, A., "Nucleation in very rapid vapour expansion" J.Chem. Phys., 19(9), 1097, 1951
[28] Plummer, P.L.M., and Hale, B.N., "Molecular models for prenucleation water clusters" J.Chem. Phys., 56, 4329, 1972.
[29] Gyarmathy, G., "Zur Wachstumsgeschwindigkeit Kleiner Flussigkeitstropfem in einer Ubersattigtm-Atmosphere" ZAMP, 14, 280, 1963.

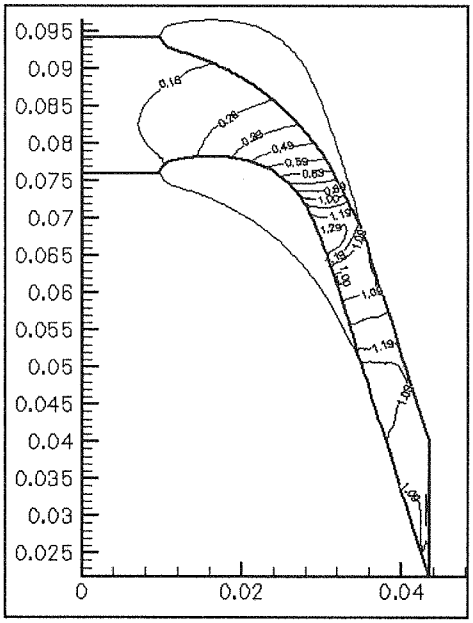

Figure (12) Constant Mach numbers in Theoretical superheated solution.

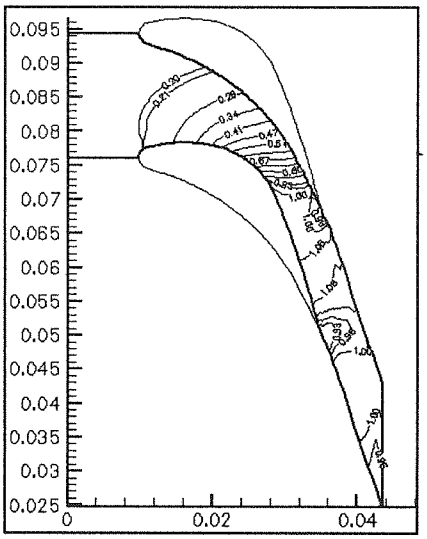

Figure (13) Constant Mach numbers in Theoretical nucleating solution.

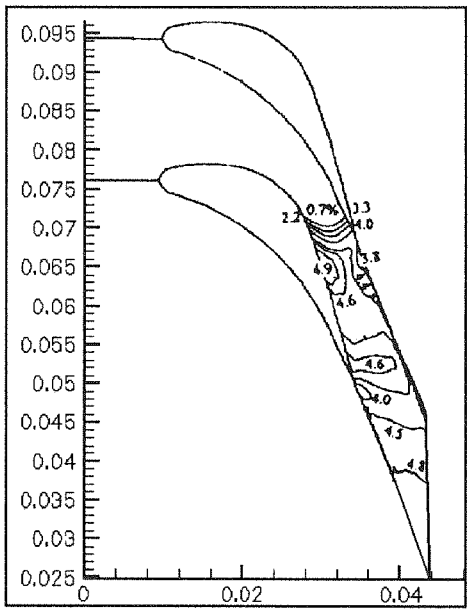

Figure (14) Constant wetness Contours in theoretical solution.

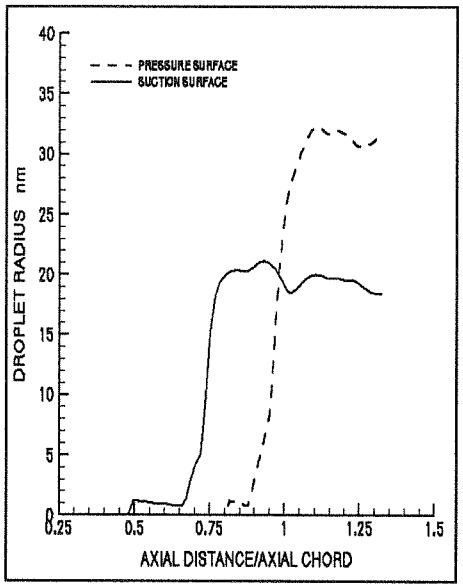

Figure (15) Calculated droplet sizes.

References

[1] Haller, B.R., Unsworth, R.G., Walters, P.T., and Lord, M.J., "Wetness measurement in a model multistage low pressure steam turbine." In proceeding of BNES Conference on Technology of Turbine Plant Operating with Wet Steam. (British Nuclear Energy Society, London). pp. 137-145. 1989

[2] Walters, P., "Wetness and efficiency measurement in L.P. turbines with and optical probe as an aid to improving performance." ASME paper 85-JPGC-GT-9, 1985.

[3] Kleitz, A., Laali, A.R., and Courant, J.J., " Fog droplet size measurement and calculation in steam turbines." In proceeding of BNES/IMechE Conference on Technology of Turbine Plant Operating with Wet Steam, (British Nuclear Energy Society, London). pp. 177-188. 1988.

[4] Tanuma, T., Sakamoto, T., "The removal of water from steam turbine stationary blades by suction slots." In proceeding of IMechE Conference on Turbomachinery. (Mechanical Engineering Publication, London) Vol. 3, paper C423/022, pp. 179-189, 1991.

[5] Dibelius, G.H., Mertens, K., Pitt, R.V., and Strauf, E., "Investigation of wet steam flow in turbines." In proceeding of IMechE Conference on Turbomachinery-Efficiency Prediction and Improvement, Cambridge (Mechanical Engineering Publication, London) C271/87, pp. 135-143. 1986-7.

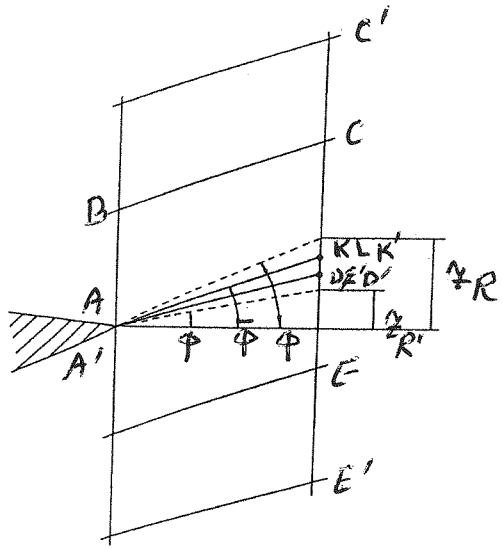

Figure (7) Illustration of modified treatment Of the downstream boundaries.

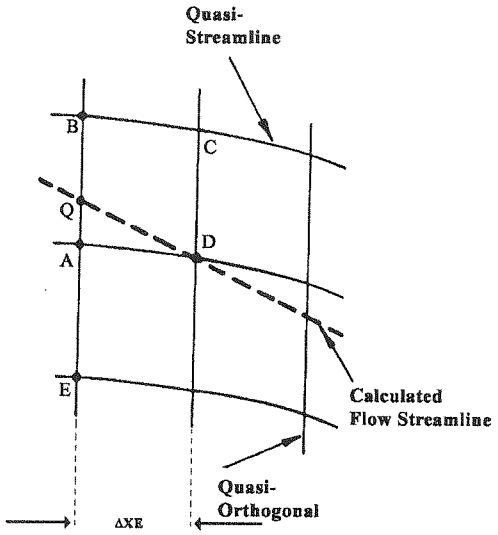

Figure (8) Details flow streamline.

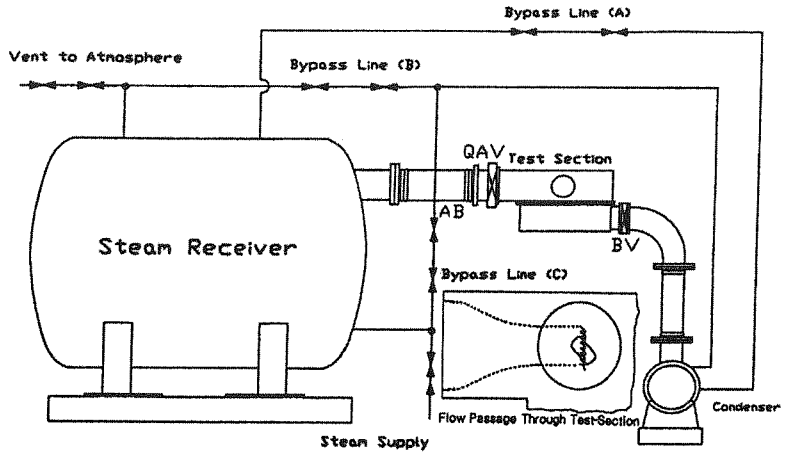

Figure (9) General arrangement blow down steam tunnel.

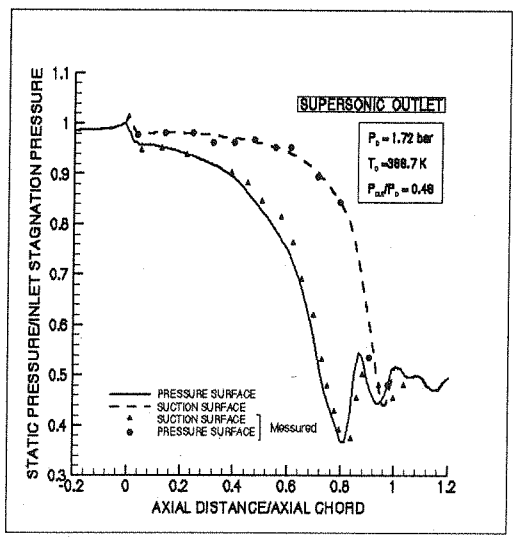

Figure (10) Theoretical and experimental pressure distributions-(superheated case).

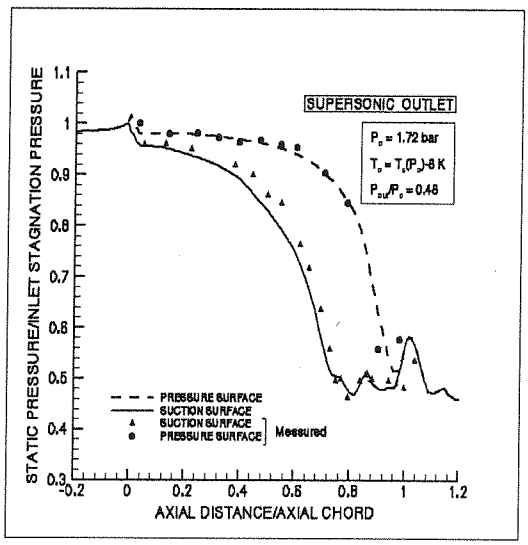

Figure (11) Theoretical and experimental pressure distributions-(nucleating case).

r	Droplet radius
t	Time
T	Temperature
$T_S(P)$	Saturation temperature at P
v	Specific volume
V_X	Component of velocity in the X direction
V_Y	Component of velocity in the Y direction
w	Wetness friction
X,Y	Cartesian coordinates
α	Heat transfer coefficient
λ	Thermal conductivity
ρ	Density
	$\rho_s(T)$ Density of saturated steam at temperature T
σ	Surface tension
ϕ	Angle made between stream line and X axis
$\underline{\omega}$	Conserved variables (vector)

Subscripts

0	Stagnation condition
G	Vapour phase
L	Liquid phase
r	Droplet of radius r
s	Saturation

Superscripts

- Critical condition

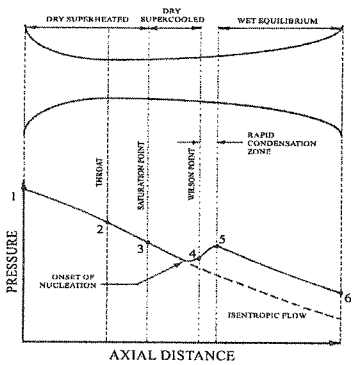

Figure (1) Axial pressure distribution in a nozzle with spontaneous condensation.

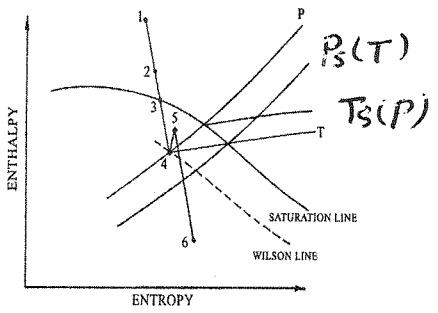

Figure (2) State line for expanding steam in a nozzle with spontaneous condensation.

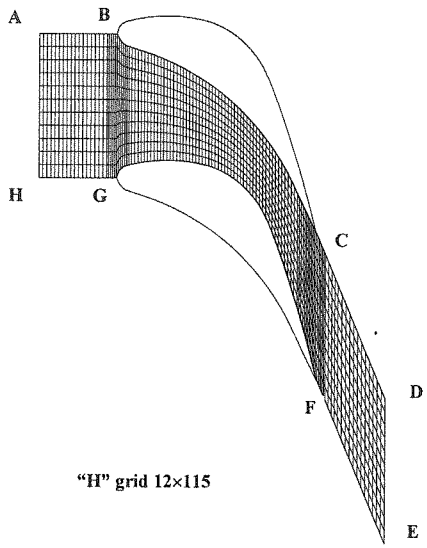

Figure (3) Blade passage and boundaries.

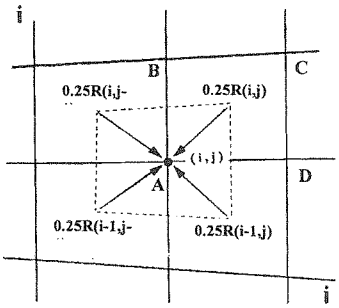

Figure (4) typical flow element & Distribution of flux residual from cell to node.

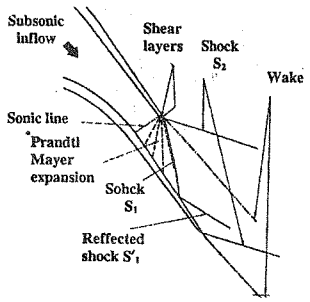

Figure (5) Transonic cascade flow structure.

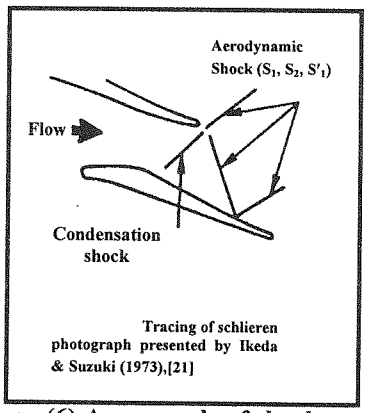

Figure (6) An example of shock wave structure in condensing steam cascades.

$$\frac{dr}{dt}=\frac{\alpha(T_L-T_G)}{\rho_L(h_G-h_L)} \tag{36}$$

where α is the heat transfer coefficient between the droplet surface and the vapour. The nucleated droplets are initially small in comparison with the mean free path of the vapour molecules ($\bar{l}$) but can grow to become large in comparison. The following expression due to Gyarmathy [28] is used in the present study to cover the entire range

$$\alpha=\frac{\lambda}{r\,(1+3.18Kn)} \tag{37}$$

Where $Kn = \bar{l}/2r$ is Knudsen number. Using equations (35) and (37) to eliminate T_L and α respectively from equation (36) yields:

$$\frac{dr}{dt}=\frac{\lambda}{(r+1.59\bar{l})\rho_L}\left(\frac{T_L-T_G}{h_G-h_L}\right) \tag{38}$$

with the surrounding vapour conditions regarded as constant, the only variables on the right-hand side of equation (38) are r, T_L and h_L. Writing h_L in terms of T_L and using equation (35) to substitute for T_L in equation (38), the resulting expression can be integrated analytically to give

$$\frac{a}{2}(r^2-r_1^2)+b(r-r_1)+c\ln\left(\frac{r-r^*}{r_1-r^*}\right)=d.\delta t \tag{39}$$

where r_1 is the initial value of r at $t=t_1$, $\delta t = t-t_1$, T_D is datum temperature and

$$a=h_G-c_L[T_S(P)-T_D]$$

$$b=(r^*+1.59\bar{l})\{h_G-c_L[T_S(P)-T_D]\}+c_L r^*[T_S(P)-T_G] \tag{40}$$

$$c=r^*(r^*+1.59\bar{l})[h_G-c_L(T_G-T_D)]$$

$$d=\left(\frac{\lambda}{\rho_L}\right)[T_S(P)-T_G]$$

Within the validity of equation (35), the above equation describes the variations of a droplet radius with time accurately. However, although analytic, because of the logarithmic term it has to solved by iteration.

Notation

B	Second Virial coefficient
c	Specific heat
F_C, G_C	Flux defined in equation(1)
G	Gibbs's free energy
h	Specific enthalpy
j	Rate of formation of new droplets per unit mass
K_n	Knudsen number = $\bar{l}/2r$
$\bar{l}$	Mean free path
L	Enthalpy of phase change
n	Number of molecules per unit mass of fluid
N	Number of droplet per unit mass
P	Pressure
$P_s(T)$	Saturation pressure corresponding to T
q	Condensation coefficient
R	Gas constant

The change in the free energy of a mass of vapour at P and T_G condensing to a liquid droplet has a maximum ΔG^* occurring at the critical radius r^*, where using an equation of state truncated at the second virial coefficient:

$$r^* = \frac{2\sigma}{\rho_L R T_G \left\{ \ln\left[\rho_S(T_G)/\rho_G\right] + 2B\left[\rho_S(T_G) - \rho_G\right] \right\}} \tag{31}$$

and

$$\Delta G^* = \frac{4}{3}\pi r^{*2}\sigma \tag{32}$$

ΔG^* presents an activation barrier to the condensation of vapour. The formation of critical droplets in a pure vapour is studied by the classical nucleation theory [23-24]. This theory has proved to be the most effective in describing the nucleation rate and still is being used by some researchers (e.g. see reference [25]). In the present investigation the nucleation theory adopted is the classical result subject to the refinements by Courtney [26] and by Kantrowitz [27]. The expression for the nucleation rate as the number of droplets formed per unit volume and time as given by the classical theory is:

$$J' = q\frac{\rho_G^{\,2}}{\rho_L}\sqrt{\frac{2\sigma n^3}{\pi}}\,.\exp\left\{ \frac{16\pi n\sigma^3}{3\rho_L^{\,2}(RT_G)^3\left\{ \mathrm{Ln}\left[\frac{P}{P_S(T_G)}\right]\right\}^2} \right\} \tag{33}$$

or per unit mass and time:

$$J = \frac{J'}{\rho_G} \tag{34}$$

Following the work of Plummer and Hale [28], the surface tension of a small cluster is taken to be that of a flat surface and the condensation coefficient is taken as unity. This combination does not entail any adjustable constants and gives good all-round agreement with experimental results over a wide range of conditions.

(b) Integration of the droplet growth equation

Once over the critical size the droplets grow by capturing mass from the surrounding vapour. The condensing molecules give up latent heat to the droplets initially, but for the droplets to grow the bulk of this energy must be returned to the vapour. For an exact calculation of the droplet growth rate the heat and mass transfer equations have to be solved simultaneously, which is numerically laborious. In the present study, to reduce the volume of algebra Gyarmathy's approximation [29] relating the droplet temperature to its radius is adopted, which is

$$T_L = T_S(P) - \left[T_S(P) - T_G\right]\left(\frac{r^*}{r}\right) \tag{35}$$

This expression is true providing the variations in the surface tension of water and of the enthalpy of evaporation in the temperature range T_G to T_L can be neglected.

With the droplet temperature determined, the thermal inertia of the droplets is regarded as small and the growth rate calculated from the energy balance, yielding:

shocks on the suction surface. The first is due to the trailing edge shock wave on the pressure surface which has extended across the passage and is reflected from the suction surface, the second is the shock wave on the suction side of the trailing edge. All the flow features have been predicted satisfactorily by the solution.

In the case of the nucleating test, the measured pressure rise at 74% axial chord length on the suction surface is due to condensation shock and occurs just downstream of the throat. The location of the rapid condensation zone is predicted slightly late and there is some smearing of the pressure change in the theoretical solution but this regarded as acceptable. It will also be seen that pressures obtained on the suction surface from the two solutions are similar before the nucleation zone beyond which the pressure in the nucleating case is consistently higher than that for the dry flow.

It is to be noted that the position and characteristics of the rapid condensation zone is in sensitive to the inlet supercooling. Downstream of the rapid condensation zone the general features associated with trailing edge shock waves are similar except that, for similar pressure ratios, Mach numbers are lower in condensing flows.

Contours of constant Mach number for the superheated and nucleating solutions are presented in Figs. 12 and 13 respectively; comparison of the constant Mach number contours shows that in the region upstream of the throat the two expansions are very similar. In the nucleating solution, the sonic line has shifted slightly downstream of the throat. Mach number at the physical minimum area is below unity indicating that the flow has choked at a velocity below the frozen speed of sound. Downstream of the throat, the detailed features of the nucleating solution differ from those of the superheated test mainly because of the lower Mach numbers in the condensing test.

Contours of constant wetness fraction in the wet solution are given in Fig. 14 and variations of mean droplet radius along the stream lines corresponding with the suction surface and pressure surface are shown in Fig.15. As expected, nucleation starts earlier on the suction surface. The steepness of rise in the droplet radius soon after nucleation is an indication of the extent of the rapid condensation zone. It will also be seen that on the suction surface the droplets evaporate immediately upstream of the trailing edge and for same distance downstream of it; this is due to the development of the shock waves which increase the vapour temperature. Beyond this with the conditions adopted the droplets begin to grow when the pressure starts to fall.

The droplets formed on the suction surface appear to be smaller than those formed on the pressure side. This is thought to be a consequence of the differences in the local rates of expansion as the different streamlines reach their limiting degrees of supercooling.

10- Summary of Conclusions

The most important characteristic of nucleating flow is the high degrees of supercooling initially attained by the fluid and the sudden release of latent heat as the system regains thermodynamic equilibrium. The resulting internal heat transfer is irreversible leading to unavoidable thermodynamic losses. The release of heat caused by rapid condensation also affects the aerodynamic behaviour of the flow. Furthermore, rates of pressure change in the different streamlines in blade to blade flows offer thermodynamic paths to the working fluid which can differ greatly. The quality of agreement between the numerical and experimental results indicate that cell vertex Jameson scheme can be applied to yield fast results with good accuracy for two-dimensional nucleating flows of steam in blading.

APPENDIX (Droplet behavior)

(a) Nucleation theory

The partial derivatives, $\partial F_1/\partial T_G$, $\partial F_1/\partial T_L$, $\partial F_1/\partial T_{s(p)}$, etc., for use in the successive iterations are obtained analytically. When the variations in droplet formation and growth rates are substantial the path between Q and D is divided into a number of subintervals and the calculations are carried out for each step.

At the end of this sequence all fluid properties including pressure temperature and enthalpy at point D have been calculated. The solution can then follow the remainder of the steps to complete the iteration. When the solution converges all the equations are simultaneously satisfied.

8- Experimental Apparatus (General Arrangement)

The general features of the equipment are shown schematically in Fig.9 The equipment is capable of generating a supply of supercooled steam. In addition, it can operate under fully superheated conditions; it thus allows the performance of profile under corresponding superheated and nucleating conditions to be compared.

The receiver is a tank of 28 m^3 capacity. To generate supercooled steam the receiver is first charged with saturated steam and than vented to the condenser. This has the effect of expanding the content to predetermined degrees of supercooling without the penalty of giving it kinetic energy. Supercooled steam thus generated then passes to the test section.

Valve (1) is a quick acting valve with a typical opening time of 70 ms and release the flow through the test section to the condenser. The opening of the quick-acting valve is followed by starting transients which then decay. Thereafter a quasi-steady flow is established in the test section which can be studied.

The test section is essentially a stainless steel fabrication which hold two cover plates 76 mm apart. The blade profiles to be investigated are mounted on circular supporting plates which fit into the test section. The profiles are based on a typical nozzle section of an operating turbine, and are of 76 mm length and 35.76mm chord. The pitch and axial chord are 18.26 and 25.27 mm respectively. The cascade consists of six blades and two half profiles forming seven passages.

The central passage is the effective test section and tapping points have been drilled into the blade surfaces either side of the central passage and into the side walls. Valve (2) is a butterfly valve and used for setting the downstream pressure.

To take surface pressure measurements during the short run times, each tapping point is connected by an oil filled stainless steel capillary tube to a separate piezo-resistive pressure transducer integral with its own amplifier. The transducers are calibrated in situ through the data acquisition system and the measurements are accurate to within $\pm$ 0.01 bar. Analogue signal from the pressure transducers are transferred to a micro computer via a data-logger unit. The temperature of steam in the tank when superheated is measured by two shielded thermocouples, but the temperature of supercooled steam cannot be measured by thermocouples directly. This is because steam condenses on the surface of the instrument and the thermocouple will indicate the saturation temperature. The procedure used for evaluating the temperature of supercooled steam is given in [22]. It is estimated that the deduced stagnation temperature of steam are to within $\pm$ 1 K.

9-Results and Discussion

The experimental observations considered are the measurements which were carried out at Birmingham University to investigate the performance of a cascade of typical blade profile of an operating turbine[10]. The theoretical and experimental surface pressure distributions for superheated and nucleating tests with supersonic outlet are compared in Figs. 10 and 11 respectively. The theoretical solution plotted in Fig. 10 is one obtained as a preliminary to the nucleating solution, it will be seen that there are two pressure rises due to aerodynamic

$$\Delta T_G = \frac{-F(T_G)}{dF(T_G)/dT_G} \tag{27}$$

Hence the corrected value of T_G is

$$T_{G(new)} = T_{G(old)} + \Delta T_G \tag{28}$$

The iteration process is carried out until the correction, ΔT_G, meets the specified tolerance of $\pm$ 0.005°K and consequently the new values of P, T_G and h_G are obtained. Once P, T_G and h_G are found, the rate of nucleation j_{st} is calculated and compared with a minimum value j'_{min} which the flow is considered to be dry.

7- Procedure for Two-Phase Flow

As already indicated, the field conservation equations apply equally to two-phase as well as single-phase fluids and with reference to Fig.8 the updating steps for density and energy at calculating point D are the same for both conditions. The main difference arises in the calculation of pressure from the known density and energy, which involves the calculation of the wetness fraction. For this purpose the droplet formation and growth equations have to be integrated, but these apply to individual fluid packages and hence must be evaluated along flow streamlines. To achieve this the streamline QD through point D is first identified. With the conditions along the station BAE already updated, the conditions at Q are calculated by linear interpolation between points immediately on either side of it along the station. The time taken for droplets to travel to the calculating point D is calculated as:

$$\delta t = \frac{\Delta X_E}{(V_{XQ} + V_{XD})/2} \tag{29}$$

The droplet radius r_Q and number per unit mass N_Q at this point are adopted as the starting conditions for the calculation of droplet growth rate along QD. However, the droplet formation and growth rates also depend on the surrounding vapour conditions. These vary between the known conditions at Q and those to be evaluated at D. Thus, adopting T_G, T_L and $T_s(P)$ as the independent variables, an initial estimate is made for these temperatures at D and the remainder of the fluid properties evaluated from them. Based on the above temperatures, an initial approximation to the radius at D, r_D is computed using Gyarmathy's approximation equation (35) in Appendix. The droplet growth procedures are then carried out. If at the end of the integration process the calculated wetness terms do not match the estimated values, new estimates are formed and the procedure repeated. For this purpose the values of energy, density and droplet radius, e_D^-, ρ_D^-, and r_D^- resulting from the integration are compared with the original estimates and the differences defined as F_1, F_2 and F_3, i.e.

$$F_1 = e_D - e'_D = \left[(1-w)h_G + wh_L - \frac{P}{\rho}\right] - e'_D$$

$$F_2 = \frac{1}{\rho_D} - \frac{1}{\rho'_D} = \left[(1-w)v_G + wv_L\right]_D - \frac{1}{\rho'_D} \tag{30}$$

$$F_3 = r_D - r'_D$$

The necessary change in the estimated values of the independent variables ΔT_G, ΔT_L, and $\Delta T_s(p)$ are calculated from F_1, F_2 and F_3 by the Newton-Raphson recursion formula.

2-With the new values of properties calculated, two points R and R′ lying along pitchline CE, are obtained as lying on the new streamlines through A and A′ respectively. The angle ϕ and ϕ' are calculated from:

$$\tan(\phi)=\frac{Z_R}{\Delta X_J}=\frac{(\rho V_y)_R}{(\rho V_x)_R} \qquad \tan(\phi')=\frac{Z_{R'}}{\Delta X_J}=\frac{(\rho V_y)_{R'}}{(\rho V_x)_{R'}} \tag{22}$$

Where the values of ρV_x and ρV_y at points R and R′ are evaluated by using interpolation through (C′, C, D) and (E′, E, D′) respectively.

3-The average angle is calculated as:

$$\bar{\phi}=\frac{1}{2}(\phi+\phi') \tag{23}$$

and a common streamline is obtained as line AK and A′K′. The properties at K and K′ are calculated by interpolation or extrapolation from the appropriate points. The calculated pressures are equalized and the values of the remaining calculated properties are adopted.

4-By adopting the new calculating points K and K′, all other points in the pitchwise direction are shifted and the properties of the new interior points are evaluated from the old points. The calculation is carried out successively downstream to the exit plane from which a new grid system is determined.

6- Procedure for Single-Phase Flow

When the steam is dry the wetness fraction is zero. Hence the overall specific enthalpy, h, is equal to h_G and ρ is equal to ρ_G and the internal energy is:

$$e = h_G - P/\rho_G \tag{24}$$

In the numerical scheme, the property resulting directly from the time stepping procedure is the internal energy, which is given by:

$$e=e_0-\frac{V_x^2+V_y^2}{2} \tag{25}$$

To calculate the pressure, P, and temperature, T_G, from the known values of e and ρ, a Newton-Raphson technique is employed as follows.

Using the known value of density and an assumed value for the temperature, an approximate value for pressure is obtained from equation of state, equation(12). The corresponding value of h_G is calculate from Eq.(15) and the specific internal energy is calculated from Eq.(24). Now, if this value for specific internal energy does not equal the value as calculated by equation(25), then the assumed temperature needs to modified. For this purpose the error $F(T_G)$ is defined as:

$$F(T_G)=\left(e_0-\frac{V_X^2+V_Y^2}{2}\right)-\left(h_G-\frac{P}{\rho_G}\right) \tag{26}$$

from which the correction to T_G is given by:

The values at the time level "n" then updated to the new time level "n+1" in the following four stages:

$$\underline{\omega}^{\circ} = \underline{\omega}^{n}$$

$$\underline{\omega}^{1} = \underline{\omega}^{0} + \alpha_1 \Delta t(\underline{R}^{0} + \underline{D}^{0}) \qquad \underline{\omega}^{2} = \underline{\omega}^{0} + \alpha_2 \Delta t(\underline{R}^{1} + \underline{D}^{0})$$

$$\underline{\omega}^{3} = \underline{\omega}^{0} + \alpha_3 \Delta t(\underline{R}^{2} + \underline{D}^{0}) \qquad \underline{\omega}^{4} = \underline{\omega}^{0} + \alpha_4 \Delta t(\underline{R}^{3} + \underline{D}^{0}) \qquad (21)$$

$$\underline{\omega}^{n+1} = \underline{\omega}^{4}$$

where Δt is the local time marching step; 1, 2, 3 & 4 refer to intermediate time step in Runge Kutta scheme and the coefficients α_1, α_2, α_3 and α_4 are 1/4, 1/3, 1/2 & 1 respectively. This scheme is fourth-order accurate in time and second-order accurate in space.

With reference to Fig.3, there are four types of boundaries. These are the inflow boundary (AH), the outflow boundary (DE), the solid wall boundaries (BC and GF), and the periodic boundaries (AB, CD, HG & FE). Inflow and outflow boundary conditions used in this study were the characteristic and extrapolation type. If the flow is subsonic there will be three incoming characteristics and one outgoing characteristic at the inflow while the opposite is true at the outflow boundary where there are three right running characteristics and one left running characteristic. By the theory of characteristics, three conditions may therefore be specified at the inflow and one condition at the outflow. The remaining conditions are numerically determined by the solution of the differential equations. The three conditions specified at the inflow are the total pressure, total temperature and the flow angle. The static pressure is extrapolated from the interior cell to the inflow. At the outflow boundary, the one physical condition specified is the static pressure. while total pressure, total temperature and flow angle are extrapolated from the interior. For supersonic flow, the static exit pressure is also extrapolated from the interior point.

On the blade surface, the "zero flux" conditions are imposed. For blade-to-blade calculations in the case of cell vertex scheme, when the flow is dry the periodicity condition on the boundary streamlines upstream and downstream of the blade row is easily satisfied by assuming that for corresponding points on each of the streamline, all properties are equal. But this procedure is questionable downstream of the trailing edge because the fluid reaching the trailing edge from the suction and pressure sides of the blade will not always have followed the same process path. For example, in the presence of a passage shock in single-phase transonic cascades as described in standard texts [20], and shown in Fig.5. The loss in total pressure and hence the properties on the suction side are different from those of the pressure side this is particularly serious in case of nucleating flows. An example of shock wave structure obtained in condensing cascade is shown schematically in Fig.6, [21].

In nucleating flows, the fluid reaching the trailing edge from the suction surface has usually nucleated while that from pressure surface is supercooled but still dry. Even in wet flows, the wetness fraction along the suction side is generally different from that along the pressure side; consequently, all other properties can differ. Under these circumstances, the only assumptions, which can be made, are that the pressures on both sides of the streamline through the trailing edge are equal and that the two streams flow in parallel directions [12]. With reference to the magnified grid system shown in Fig. 7, the properties at two typical points D and D′ are calculated in the following steps:

1-The two lines AD and A′D′ are the estimated streamlines downstream of the trailing edge from the previous iteration. The values of all properties at D and D′ are obtained by assuming that AD and A′D′ are solid boundaries.

const. = 1782.24 in SI units

The above system of equations is sufficient to describe the flow completely.

5- Numerical Arrangement & Boundary Conditions

The mesh adopted is shown in Fig. 3 and an enlarged view of a typical flow element ABCD is illustrated in Fig. 4.

Development of the solution procedure is based on the Jameson's fourth order Runge Kutta numerical integration using cell-vertex formulation in which the flow variables are stored at cell vertices A,B,C and D. It has been shown by Martinelli [15], Dick [16], Swanson and Radespiel [17], amongst others that cell-vertex formulation offers some advantages over the cell-centered one. Since the variables are piecewise linear over the cell face, the formulation is second-order accurate in space irrespective of the irregularity of the grid. For a uniform mesh, these would be no difference between the cell-centered and cell-vertex scheme, however, cell-vertex storage does not require extrapolation to the solid boundary to obtain the wall static pressure which is necessary in solving the momentum equations for cells adjacent to the solid boundary. Therefor, this scheme yields fast results with good accuracy [18].

To calculate the change at the calculating points from those for the cell, approximation of Eq.(1) is applied to each cell separately; For example considering the inviscid fluxes Fc and Gc of a conserved variable, ρ , the right hand side of the continuity equation can be evaluated by:

$$R_{ij}(\rho) = -\frac{1}{\Omega_{ij}} \oint (F_{cij}(\rho)dy - G_{cij}(\rho)dx) \tag{17}$$

where, Fc (ρ) = ρV_X and Gc (ρ) = ρV_y. This procedure leads to a system of ordinary differential equations of the form

$$\left(\frac{\partial \underline{\omega}}{\partial t}\right)_{ij} = R_{ij}(\underline{\omega}) \tag{18}$$

Where $R_{ij}(\underline{\omega})$ represents the sum of inviscid residuals. The calculated changes in $\underline{\omega}_{ij}$ apply to the values of properties within the cell, whereas, the variables are actually stored at the nodes. Consequently, they have to be redistributed to the four surrounding nodes. This maybe done simply by sharing the changes equally between the four cells as shown in Fig.4. Hence,

$$R_A(\underline{\omega}) = 0.25[R_{ij}(\underline{\omega}) + R_{i-1,j}(\underline{\omega}) + R_{i,j-1}(\underline{\omega}) + R_{i-1,j-1}(\underline{\omega})] \tag{19}$$

Thus, the scheme is symmetrical in space and the equivalent discretized equation for node A will be:

$$\left(\frac{\partial \underline{\omega}}{\partial t}\right)_A = R_A(\underline{\omega}) + D_A(\underline{\omega}) \tag{20}$$

$D_A(\underline{\omega})$ is the added artificial dissipative term to suppress numerical instabilities, The artificial dissipative term used in the present work, is that proposed by Jameson et al.[19] modified to suit the cell-vertex formulation. This is a blend of second and fourth order terms with a pressure switch to detect changes in pressure gradient.

Equation (20) is integrated with respect to time using the modified four-stage Runge Kutta time stepping scheme in which the dissipative terms are frozen at the values of the first stage.

The additional information necessary requires equations to describe the properties of the liquid and vapour phases; The specific volume of saturated water, v_L is obtained from Keenan and Keyes:

$$v_L = \frac{v_C + a(T_C - T_S)^{1/3} + b(T_C - T_S) + c(T_C - T_S)^4}{1 + d(T_C - T_S)^{1/3} + e(T_C - T_S)} \qquad (10)$$

where v_c is the critical specific volume of 3.1975 cm^3/g, T_C is the critical temperature of 647.27° K and

$a = -0.3151548$ $\quad b = -1.203374*10^{-5}$
$c = 7.48908*10^{-13}$ $\quad d = 0.1342489$
$e = -3.946263*10^{-3}$ in SI units

The specific enthalpy of water at temperature T_L may be written with sufficient accuracy as:

$$h_L = c_L (T_L - T_D) \qquad (11)$$

where T_D is datum temperature taken as 273.15° K.
The equation of state adopted for the vapour phase is:

$$P = \rho_G RT_G(1 + B\rho_G) \qquad (12)$$

where B is the second Virial coefficient and thermodynamic properties of steam are calculated from mutually consistent relationships.
From the first and second laws of thermodynamics and by using Maxwell's relations it can be shown that,

$$\left(\frac{\partial h_G}{\partial P_G}\right)_{T_G} = v_G - T_G\left(\frac{\partial v_G}{\partial T_G}\right)_P \qquad (13)$$

Integration of above equation gives:

$$h_G = \int\left[v_G - T_G\left(\frac{\partial v_G}{\partial T_G}\right)_P\right]dP + F_h(T_G) \qquad (14)$$

After introducing the equation of state the final expression for enthalpy of dry steam is:

$$h_G = \frac{RT_G}{2}\left(\sqrt{1 + \frac{4PB}{RT_G}} - 1\right)\left(1 - \frac{T_G}{B}\frac{dB}{dT_G}\right) + F_h(T_G) \qquad (15)$$

It may also be shown that:

$$F_h(T_G) = a\ln T_G + bT_G + cT_G^{\,2} - dT_G^{\,3} + eT_G^{\,4} - fT_G^{\,5} + \text{const.} \qquad (16)$$

where
$a = 46.0$ $\quad b = 1.47276$ $\quad c = 0.419465*10^{-3}$
$d = 7.33297*10^{-8}$ $\quad e = 6.16548*10^{-11}$ $\quad f = 1.94063*10^{-14}$

the above conservation equations apply to single-and two-phase fluid as long as in the latter case ρ and h refer to overall vapour and liquid mixture.

3- Application to Two-Phase Flows

In the case of two-phase flows, the main influence of phase change is the release of latent heat, which directly affects the energy equations. To deal with this aspect of the problem, the wetness fraction is defined as:

$$w = \frac{\text{(mass of liquid)}}{\text{(mass of vapour) + (mass of liquid)}} \tag{5}$$

The approach is to regard wet steam as the summation of a large number of spherical droplets of specified size and the vapour phase of given pressure and temperature which fills the space between them and because the radii of droplets nucleated spontaneously in turbines is very small, it is customary to assume that they follow the vapour path line exactly with zero velocity slip. The system as a whole must obey the conservation laws. To apply the conservation equations to two-phase flows they have to be combined with equations (33) and (36) in appendix describing droplet formation and growth and solve simultaneously. An important difference between the two families of equations is that those describing droplet formation and growth are stiff and have to be integrated over much shorter time intervals. In addition, the droplet growth equations are more naturally expressed in Lagrangian rather than Eulerian form and droplets are assumed to be carried along streamlines which do not necessarily concid with the grid lines. For these reasons the two sequences of calculations are carried out separately, but it is essential that the coupling between them be exact. This is achieved by the introduction of the wetness fraction, w, into the expressions for mixture enthalpy, h, and density, ρ, to yield:

$$h = wh_L + (1-w)h_G \tag{6}$$

and

$$1/\rho = w/\rho_L + (1-w)/\rho_G \tag{7}$$

Where the suffixes G and L refer to vapour and liquid phases respectively. The wetness fraction may be expressed as:

$$w = \frac{4}{3}\pi \bar{r}^3 \rho_L N \tag{8}$$

where N is the number of droplets per unit mass of the mixture. The total number of droplets at the end of each calculation step is the sum of the number of droplets existing in the flow at the beginning of the step, N_1 and the number formed by nucleation over the time increment δt, i.e.

$$N = N_1 + J\delta t \tag{9}$$

At the end of the calculation the two populations of droplets, i.e. the newly formed ones and those existing in the flow, are combined into one population and the mean radius $\bar{r}$ calculated on an r.m.s basis.

The investigation is undertaken as a contribution to a better understanding of these problems. The development of nucleation theory has been help ful in studying the wetness problems in turbines, as the equations describing droplet formation and growth can be combined with the standard gas dynamic conservation equations to form a set and treated numerically [6-11].

One particular difficulty in dealing with two-phase flows over turbine blading is that in general these problems involve both sub and super sonic flows with appreciable transonic sections while the speed of sound in these mixtures is not explicit and depends on the local conditions and the form of the governing equations differ in sub-tran and super sonic flows. Under these circumstances, the most suitable way of treating the equations is the time marching technique. In addition, it was found in earlier investigations that wet steam calculation methods are not only extremely time-consuming but also tend to suffer from numerical stability problems usually traceable to the mathematical stiffness of the governing equations [12]. Hence, if these techniques are to become standard design tools of industry, there is obviously a need for developing faster and less temperamental programs. In this paper one such procedure for calculating two-dimensional cascade flow is described. It is based on the Jameson finite–volume time marching method for single phase flows [13], but departs from tradition in the treatment of the wetness terms by introducing a novel method for integrating the combined energy and droplet growth equations. This procedure which explained in appendix reduces the volume of algebra drastically [14].

2- General Flow Equations

Considering unsteady, inviscid two-dimensional compressible flow of a vapour carrying a population of droplets with no interphase slip, the conservation equations of mass, momentum and energy in integral form applied to a flow element may be written as:

$$\Omega\frac{\partial \underline{\omega}}{\partial t} = -\oint[\underline{F_c}dy - \underline{G_c}dx] = 0 \tag{1}$$

Where Ω is a fixed area of computational cell, $\underline{\omega}$ represents the conserved variables, $\underline{Fc}$ and $\underline{Gc}$ are the fluxes in x and y directions. These vectors may be expressed as:

$$\underline{\omega} = \begin{bmatrix} \rho \\ \rho V_x \\ \rho V_y \\ \rho e_0 \end{bmatrix} \quad , \quad \underline{F_C} = \begin{bmatrix} \rho V_x \\ \rho V_x^{\,2} + P \\ \rho V_x V_y \\ \rho V_x h_0 \end{bmatrix} \quad , \quad \underline{G_C} = \begin{bmatrix} \rho V_y \\ \rho V_y V_x \\ \rho V_y^{\,2} + P \\ \rho V_y h_0 \end{bmatrix} \tag{2}$$

Here, e_0 and h_0 are the total energy, and total enthalpy; where:

$$e_0 = h_0 - \frac{P}{\rho} \tag{3}$$

and

$$h_0 = h + \frac{V_x^{\,2} + V_y^{\,2}}{2} \tag{4}$$

An Investigation of Two-Dimensional, Two-Phase Flow of Steam in a Cascade of Turbine Blading by the Time-Marching Method

A. R. Teymourtash
Ph.D Student

M. R. Mahpeykar
Assistant professor

Mechanical Engineering Department,
Ferdowsi University of Mashhad

Abstract

During the course of expansion in turbines, the steam at first supercools and then nucleated to become a two-phase mixture. This is an area where greater understanding can lead to improved design. This paper describes a numerical method for the solution of two-dimensional two-phase flow of steam in a cascade of turbine blading; the unsteady Euler equations governing the overall behaviour of the fluid are combined with equations describing droplet behaviour and treated by Jameson's fourth order Runge Kutta time marching scheme which modified to allow for two-phase effects. The theoretical surface pressure distributions, droplet radii and contours of constant wetness fraction are presented and results are discussed in the light of knowledge of actual surface pressure distributions.

Keywords

Cascade, Jameson, Nucleation, Steam, Turbine, Supercooling, Time marching, Two-phase flow.

1- Introduction

A broad spectrum of flow conditions are encountered at various stages of a modern steam turbine. Conventionally, the condensation process in a transonic cascade of turbine blading is considered to be directly analogous to that observed in Laval nozzles operating at transonic speeds. A typical expansion of steam in a convergent divergent nozzle is shown in Figs.1 and 2. Initially superheated steam (1) is expanded to sonic line and droplet embryos begin to form and grow in the vapour. The rate of formation of these embryos is low and the steam continuous to expand as a dry single vapour phase in a metastable, supercooled or supersaturated state. Depending on the local conditions the nucleation rate increases dramatically and reaches its maximum at the Wilson point (4) which occurs after the throat and is also the point of maximum supercooling. This process is termed "homogeneous nucleation". From (4) to (5) the fluid condenses experiencing the associated pressure rise (condensation shock) caused by the release of latent heat to the supersonic stream. At the end of this zone nucleation ceased and the number of droplets present in the flow remains constant. From (5) to (6) the expansion takes place close to equilibrium.

Many investigations into the behaviour of flowing wet steam in turbines have been reported [1-5]. A tangible wetness effect is the erosion of blading but this is only one consequence of the presence of water in steam. More serious are the problems caused by local departures of the system from thermodynamic equilibrium. This is because the release of latent heat associated with return to equilibrium can affect the behaviour of the parent vapour; choking mass flow rate and the change of flow patterns around the blades are two specific examples.